PCCP

Accepted Manuscript

This is an *Accepted Manuscript*, which has been through the Royal Society of Chemistry peer review process and has been accepted for publication.

Accepted Manuscripts are published online shortly after acceptance, before technical editing, formatting and proof reading. Using this free service, authors can make their results available to the community, in citable form, before we publish the edited article. We will replace this *Accepted Manuscript* with the edited and formatted *Advance Article* as soon as it is available.

You can find more information about *Accepted Manuscripts* in the Information for Authors.

Please note that technical editing may introduce minor changes to the text and/or graphics, which may alter content. The journal's standard Terms & Conditions and the Ethical guidelines still apply. In no event shall the Royal Society of Chemistry be held responsible for any errors or omissions in this *Accepted Manuscript* or any consequences arising from the use of any information it contains.

ROYAL SOCIETY OF CHEMISTRY

www.rsc.org/pccp

Cite this: DOI: 10.1039/c0xx00000x

www.rsc.org/xxxxxx

ARTICLE TYPE

DNA mediated assembly of Quantum Dot-Protoporphyrin IX FRET Probe and Effect of FRET Efficiency on ROS Generation

Seema Singh,[a] Anirban Chakraborty,[b] Vandana Singh,[a] Aniruddha Molla,[a] Sahid Hussain,[a] Manoj K. Singh[c,*] and Prolay Das[a,*]

Received (in XXX, XXX) Xth XXXXXXXXX 20XX, Accepted Xth XXXXXXXXX 20XX
DOI: 10.10

Photodynamic therapy (PDT) involves generation of Reactive Oxygen Species (ROS) by the irradiation of a photosensitizer. Controlled and targeted release of ROS by a photosensitizer is crucial in PDT. For achieving controlled generation of ROS, a ZnSe/ZnS quantum dots (QDs) donor and protoporphyrin IX (Pp IX) acceptor based fluorescence resonance energy transfer (FRET) probe is reported here. The QDs and Pp IX are assembled either by direct conjugation or through DNA hybridization. Complementary DNA strands are individually conjugated to the QDs and Pp IX by amide coupling. Due to the overlap of the emission spectrum of QDs and the absorption spectrum of Pp IX, efficient transfer of energy from QD to Pp IX was observed in both the cases. The FRET efficiency was quantitatively evaluated by steady-state and time-resolved spectroscopy and compared between QD-Pp IX direct conjugate and QD-DNA-Pp IX assembly at various donor to acceptor ratio. Since a single QD can harbor multiple number of Pp IX-DNA counterpart through DNA hybridization, FRET efficiency was found to increase with the increase in the number of Pp IX acceptors. ROS generation from Pp IX was studied for the FRET pairs and was found to be affected by the irradiation time of the QD donor.

1. Introduction

In biomedical research, there is a constant effort to combine diagnostics with therapy. While the diagnostics elements ensure early detection, simultaneous therapy provides instant remedy and thus minimizes future complications by saving invaluable time.[1] The main goal of such research is to develop small probes with high selectivity, stability and capacity to detect ailments and deliver the right dosage of drug in the desired tissues at the same time.[2] In this aspect, semiconductor quantum dots (QDs) have received significant recognition in biomedical research, in particular as the diagnostics handle for molecular sensing and cellular imaging.[3-5] The size and material dependent properties of semiconductor QDs have been used successfully in biosensing, immunoassay, drug delivery, thin film solar cell, light emitting diode, as laser materials and others.[6-9] Multicolour imaging and cancer targeting using QDs have also been reported.[10-12] One of the less researched and scarcely explored areas of the application of QDs is their uses in photosensitization for Photodynamic therapy (PDT) of cancer. PDT has been successful in addressing certain types of cancer including esophageal cancer and non-small cell lung cancer.[13, 14] The FDA approved photosensitizers (PS) Photofrin®, 5-aminolevulinic acid (5-ALA), a precursor of Protoporphyrin (Pp IX) have been used to generate Reactive Oxygen Species (ROS) upon irradiation.[15, 16] The ROS kills the cancer cells following their accumulation in the concerned tissues.

The use of QDs in PDT can be very advantageous since apart from being a photobleaching resistant detection probe, it enables the use of a wavelength where the photosensitizer does not absorb, thus offering flexibility to utilize variable excitation wavelengths to activate the photosensitizer molecule.[17] CdSe QDs when excited have been shown to excite phthalocyanine photosensitizer (Pc4) by FRET to generate ROS.[18] Generation of singlet oxygen on excitation at 488 nm via thiol-capped CdTe QDs-sulfonated aluminum phthalocyanine composites have also been reported.[19]

One potential shortcomings of Cd based QDs for biological application is the toxicity issue[20] and PDT is no exception. In PDT, the toxicity of the donor and the photosensitizer in the absence of light is strictly unwarranted. DNA strand breakage and damage have also been observed in plasmids photosensitized by CdSe−ZnS QDs, that may limit their uses in PDT.[21] Previous studies have shown that engineered nanoparticles like carbon nanotubes (CNT), silver nanoparticles, CdSe QDs and TiO_2 nanoparticles can also cause lung damage by inflammatory effects when used as carrier of PS in PDT.[22, 23]

Apart from the criterion that needs to be fulfilled for an ideal donor in PDT applications including photostability and toxicity issue, it is important that the PDT system be well targeted for *in-vivo* applications. Targeting of therapeutic drugs is often done by attaching a biological entity to the drug molecule,

Physical Chemistry Chemical Physics Accepted Manuscript

which can recognize its counterpart and accumulate in the region of interest.[24] This minimizes side effects, favorably modify the dose rate and increase drug efficacy.[25, 26] It is well known that cancer cells are deficient in antioxidative defense system and hence are highly vulnerable to ROS.[27, 28] In PDT, the main concept is ROS generation and subsequent cancer cell destruction through it. However, excess ROS generation can have several side effects, whereby healthy cells can be affected. Thus, controlled and targeted release of ROS by PS is the essential need of PDT. Targeting of PDT systems with antibodies and homing peptides have been reported.[29-31] It remains to be seen whether the attaching of targeting biological entity to the donor/photosensitizer, compromises the efficiency of the PDT system or lead to controlled and sustained ROS generation.

Herein, we report the generation of ROS from Pp IX, where the excitation of the same is achieved by FRET from the ZnSe/ZnS QDs (scheme 1). Further, a comparative study of the efficiency of ROS generation for various systems consisting of the QDs and Pp IX is presented. The ROS generation from free QDs and Pp IX system (individually or in mixtures) in solution are compared with QD-Pp IX covalent conjugate (QD covalently attached to Pp IX), QD-DNA, and Pp IX-DNA individually or self-assembled by DNA hybridization. Single strand DNA (ssDNA) was attached to QDs by amide coupling. Similar chemistry was also used for covalent attachment of Pp IX to ssDNA that is complementary to the DNA sequence used to link with the QDs. Controlled and proportional release of ROS in the case of QD-DNA-Pp IX assembly was observed.

The self-recognition property of DNA has been used to assemble the QD-DNA and Pp IX-DNA conjugates. Our study shows that DNA can be used as a self-assembling molecule, whereby FRET efficiency can be modulated by careful choice of the sequence length. Moreover, deliberate choice of the sequence of DNA can provide the targeting handle, as in the case of protein recognition by DNA aptamer sequences.[32]

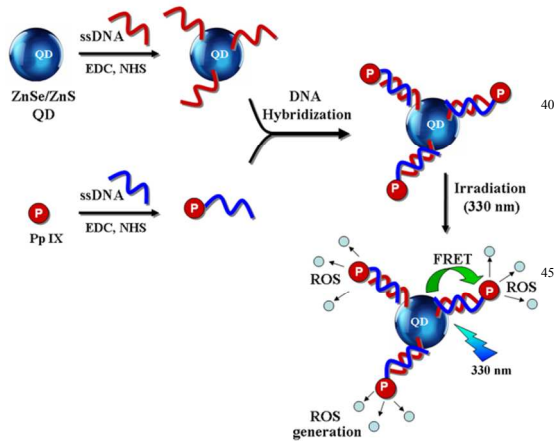

Scheme 1: Scheme for conjugation of DNA with QD and Pp IX and subsequent generation of ROS from Pp IX by FRET from QD conjugated through DNA assembly.

2. Experimental Section

2.1. Material and Methods

Selenium powder, sodium borohydride, N, N-dimethylformamide (DMF), Pp IX, dihydrorhodamine 123 (DHR 123) and 5'-amine terminated (C_6 linker) oligonucleotide DNA (12mer) were purchased from Sigma Aldrich. Zinc acetate dihydrate (Zn $(OAc)_2$•$2H_2O$), L-glutathione (GSH), 3-mercaptopropionic acid (MPA), N-hydroxysuccinimide (NHS) and 1-(3-dimethylaminopropyl) -3-ethylcarbodiimide hydrochloride (EDC.HCl) were obtained from Alfa Aesar. All chemicals were used as received. Nanopure water from Millipore was used in all experiments.

2.2. Synthesis of ZnSe/ZnS Core/Shell Quantum dots

ZnSe/ZnS QDs were synthesized by the reaction of zinc acetate and sodium hydrogen selenide. Sodium hydrogen selenide was prepared by dissolving $NaBH_4$ (15 mg, 0.4 mmol) in 1 ml of ice cold water, followed by addition of Se powder (16 mg, 0.2 mmol) under a nitrogen atmosphere. $Zn(OAc)_2$•$2H_2O$ (44 mg, 0.2 mmol) and L-glutathione (123 mg, 0.4 mmol) were dissolved in 50 ml water and the pH of resulting solution was adjusted to 10.5. The reaction mixture was deaerated and 500 µl of NaHSe (0.1 mmol) was added to the reaction mixture and exposed to microwave irradiation at 120 °C for 10 min in a Biotage Microwave reactor. MPA (106 mg, 1 mmol) and Zn $(OAc)_2$•$2H_2O$ (55 mg, 0.25 mmol) was added to the ZnSe (0.05 mmol) core solution at pH 10.5 for shelling and again exposed to microwave irradiation at 120 °C for 10 min. QDs were purified by using excess of ethanol followed by centrifugation to remove unconjugated ligands .

.

2.3. Dynamic light scattering (DLS) studies

Hydrodynamic radii of QDs were measured by dynamic light scattering on a Delsa™ Nano particle analyzer (Beckman Coulter). A solution of QDs was filtered through 0.2 micron filters for light scattering experiments. A total of 5-accumulation numbers with 75 s duration were used for data acquisition and all measurements were repeated for 5 times.

2.4. Conjugation of QD with Pp IX

EDC solution (5 µL, 10 µM) was added to Pp IX (5 µL, 1 nM) solution in DMF followed by the addition of NHS solution (10 µL, 20 µM). The reaction mixture was thoroughly mixed and allowed to stand at room temperature for 1h. To this solution, QDs (20 µL, 1 nM) were added and the reaction was heated at 55 ºC overnight. The excess of EDC and NHS were removed as the supernatant after centrifugation at 10,000 rpm. A total of four reactions were done by varying the concentration of Pp IX from 1 nM to 4 nM.

2.5. Conjugation of QD and Pp IX with DNA and self-assembly

Carboxyl terminated QDs (20 µL, 1 nM) was activated by EDC (10 µL, 10 µM) and NHS (20 µL, 20 µM) in 20 µl of 1:1 ethanol (50 %): sodium phosphate buffer (200 mM) at pH 6 with occasional sonication for a few seconds. The solution was centrifuged at 14,000 rpm for 10 min and the supernatant was discarded. The resulting pellets were washed with water,

Physical Chemistry Chemical Physics Accepted Manuscript

followed by the addition of of amine terminated ssDNA (S1) (10 µL, 5 nM). The reaction mixture was stirred for 3 h at 4 °C. Excess of EDC, NHS and unreacted DNA were removed by dialysis (MWCO-5KDa).

For the coupling of Pp IX with DNA, Pp IX in (25 µL, 5 nM) DMF was added to a premixed solution of EDC (10 µL, 25 µM) and NHS (20 µL, 50 µM) and the reaction mixture was adjusted to pH 8 by sodium bicarbonate buffer with gentle stirring for 1 h. Amine terminated ssDNA (S2) (10 µL, 5 nM) was added to the reaction mixture and stirred overnight at 55 °C. Excess of EDC and NHS was removed by dialysis (MWCO-5 KDa). The desired product Pp IX-DNA *i.e.* Pp IX-S2, Pp IX linked to a single DNA strand (S2) was purified by polyacrylamide gel electrophoresis (PAGE). The purified Pp IX-DNA was subjected to molecular weight determination by Autoflex II MALDI-TOF-MS (Bruker Daltonics, Billerica, MA) using linear negative mode. Data processing was performed by Flex Analysis software.

The QD-DNA conjugate was added to the Pp IX-DNA conjugate in sodium phosphate buffer (10 µL, 10 nM) at pH 7.5. The solution was annealed by heating at 90 °C for 10 min and slowly cooled down to room temperature. The hybridization was done separately with QD-DNA conjugate with various ratios of Pp IX-DNA conjugate from 1:1 to 1:4 with increment of 1 nM of the latter.

2.6. Gel Electrophoresis

PAGE: Conjugation of Pp IX-DNA was confirmed by 30% denaturing PAGE, run in 1X tris taurine EDTA (TTE) buffer at 200 V and imaged without any staining by a Canon D600 digital camera. Gel images were also acquired with a CCD camera using UVP gel documentation system for quantitative evaluation. The band corresponding to a single DNA strand attached to a Pp IX molecule was excised from the gel and extracted with gel elution buffer (0.5 M NH_4OAc, 10 mM $Mg(OAc)_2$, 1.0 mM EDTA and 0.1% SDS).

Agarose Gel Electrophoresis: QD-DNA (QD-S1), QD-Pp IX conjugate and QD-DNA-Pp IX (QD-S1-S2-Pp IX) assembly was visualized by 1% agarose gel electrophoresis in 1X tris acetate EDTA (TAE) buffer.

2.7. Optical Absorption and Emission Spectroscopy

For atomic absorption spectrometry (AAS), vacuum dried pellets of QD was treated with aqua regia and diluted with water. Concentration of zinc was determined by flame AAS and selenium was determined by graphite furnace AAS in a GBC 906 Atomic Absorption Spectrometer (GBC Scientific Equipments, USA).

UV-Visible spectra were recorded on an UV-2550 spectrophotometer (Shimadzu). Steady-state fluorescence spectra were collected on a Fluoromax-4 spectrofluorometer (Horiba, Japan). For excited state lifetime measurement FluoTime 200 from PicoQuant, Germany working on time correlated single photon counting (TCSPC) technique has been used. All measurements were done in water as a solvent.

For ROS measurement 5 nM dihydrorhodamine 123 solutions (20 µl) were added to a fixed volume of sample solutions and irradiated with a UV lamp (λ_{max} = 302 nm). Generation of fluorescent rhodamine 123 due to oxidation by ROS is monitored at different time interval by UV-Visible and steady-state fluorescence spectroscopy.

For the determination of quantum yield, solution of quinine sulphate (QY = 0.55) in 0.5 M H_2SO_4 was used as standard. Solution of QD and standard were prepared in such a way that their absorbance is nearly equal at the wavelength of excitation. Quantum yields were calculated using equation (1).

$$QY_x = QY_s \times (A_s/A_x) \times (I_x/I_s) \times (n_x^2/n_s^2) \quad (1)$$

Here, subscripts x and s refer to the sample and the reference material respectively, QY-Quantum yield, A - Absorbance at the excitation wavelength, I - Integrated fluorescence intensity and n - refractive index of the solvent.

3. Results and Discussion

3.1. Synthesis, Characterisation and Optical Properties of Water Soluble QDs

Synthesis of QDs in aqueous phase by conventional method is a slow process as it takes long heating time with inefficient heat transfer to the reactants. Microwave assisted aqueous synthesis of ZnSe/ZnS QDs is a rapid method where homogeneous heating of precursors can occur. Aqueous synthesis of ZnSe/ZnS QDs with dual stabilizing agents GSH and MPA was achieved by microwave heating following the procedure reported by Qian *et al.* with some modifications.[33] Molar ratio of Zn:Se was kept at 2:1 as Zn precursors have low reactivity towards NaHSe.[34] The two stabilizing agents containing –SH, –COOH and $–NH_2$ functional groups possess a lone pair of electrons that can influence the nucleation, growth and stabilization of ZnSe/ZnS QDs and might impose a kinetic barrier for the growth because of columbic repulsion. The ZnS shell on the core of ZnSe is formed by the thermal decomposition of MPA ligand that releases S^{2-} reacting with zinc source.[35] Such an effect improves surface passivity that can result in the increased fluorescence intensity. Excess of MPA was used to avoid possible formation of new nucleation of ZnS or ZnO nanocrystals.

The optical characteristics of QDs were investigated by UV-Visible and fluorescence spectroscopy. It can be seen that the QDs have broad absorption in the UV region and the first absorption peak is at 343 nm (Fig. 1A). The effective mass model equation (equation 2) was used to calculate the size of QDs.

$$E = E_g + \left(\frac{h^2}{8R^2}\right) \times \left(\frac{1}{m_e} + \frac{1}{m_h}\right) \quad (2)$$

Where E is the band gap energy of QDs, Eg is the band gap energy of bulk ZnSe, m_e and m_h are the effective masses of the electron and hole in ZnSe. The average particle size *R* of ZnSe core QDs was estimated to be 4.58 nm. Concentration of Zn and Se were determined from the AAS measurements and volume of QD was calculated. From these, the molar concentration and the total concentration of QD per liter were estimated. The average

Physical Chemistry Chemical Physics Accepted Manuscript

hydrodynamic radii of the core/shell QDs were found to be ~12 nm as measured from DLS.

The fluorescence spectra of ZnSe core and ZnSe/ZnS core/shell QD is shown in Fig. 1B. The emission spectrum shows two components: a relatively narrow peak at 373 nm which is due to the band edge emission and the broad one at 450 nm resulting from trap state emission.[36] These two components have significance in FRET as the band edge emission (λ_{max} = 373 nm) overlaps with the soret band of Pp IX and the trap state emission (λ_{max} = 450 nm) overlaps with the Q bands of Pp IX.[37] The Forster distance for this FRET probe *i.e.* QD donor and Pp IX acceptor was estimated to be 4.85 nm. Evidently, the QDs fulfill the criteria of a good donor for FRET to occur with Pp IX as an acceptor. Due to the higher fluorescence quantum yield, ZnSe/ZnS core/shell QD (QY = 0.32) was preferred over ZnSe core QD (QY = 0.19) for further investigation.

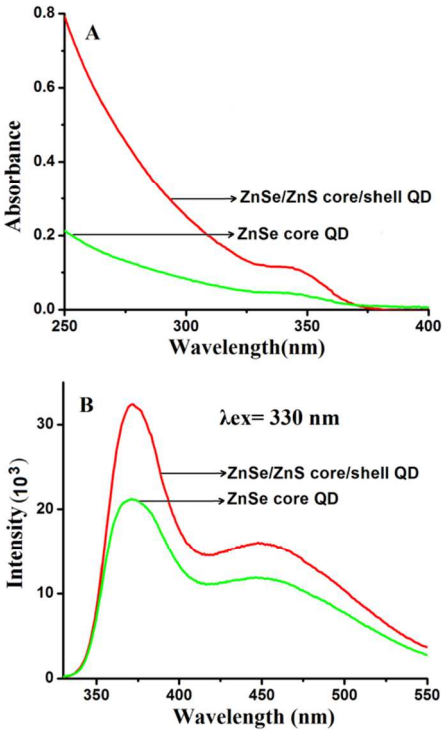

Fig. 1 **A.** UV-Visible absorption and **B.** Fluorescence Spectra of ZnSe core and ZnSe/ZnS core/shell QDs.

3.2. Synthesis, characterization of QD-Pp IX direct Conjugate and self assembly of QD-DNA and Pp IX-DNA conjugate

Water-soluble EDC and NHS are employed often for the activation of –COOH groups used in cross-coupling reactions.[38] The –COOH group of Pp IX was activated using EDC and NHS and directly conjugated to the amine group of QDs. The conjugation of QDs with Pp IX was confirmed by 1% agarose gel electrophoresis (Fig. 2). Due to the emission of the QD and Pp IX, no staining was required to visualize the samples. From gel image it can be seen that QD-Pp IX direct conjugate shows less mobility as compared to the QDs alone. Also, due to the quenching by Pp IX, the QDs' fluorescence is subdued in that sample in the gel. Yield of the reaction of QD with Pp IX was calculated from the absorption spectra of Pp IX before and after reaction in DMF-water reaction mixture solvent. From absorption studies of the Pp IX in free and conjugated state, the efficiency of the reaction of the QD with Pp IX was roughly estimated and found to decrease from ~88% to ~72 % for the reactant ratio of QD: Pp IX from 1:1 to 1:4 ratio respectively. Thus, 1:1 and 1:4 ratio of QD to PpIX yield product where QD: Pp IX were in ratio of 1:0.88 and 1:2.88 respectively. Similar approach was undertaken for yield calculation of QD-DNA-Pp IX complex.

Following the EDC-NHS mediated amide formation chemistry, two separate yet complementary 12 base long ssDNA (S1 and S2, table 1) are covalently conjugated to QDs and Pp IX. The activated ester formed from the –COOH groups of the ligands in the QDs and the Pp IX are coupled with the 5'-amine terminated ssDNA S1 and S2 respectively, following standard procedure.

Table 1: Oligomer sequences used in the study. S1 and S2 are self complementary.

S1	NH_2- 5'-TCA GTC AAC AGC -3'
S2	NH_2 - 5'-GCT GTT GAC TGA -3'

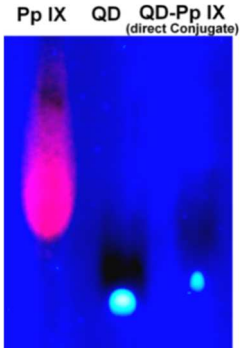

Fig. 2 1% Agarose Gel Electrophoresis showing mobility of Pp IX, ZnSe/ZnS QD and QD-Pp IX = 1:4 Conjugate.

Due to the presence of multiple –COOH functional groups on the surface of the QDs, more than one ssDNA can be attached to the QD. This is indeed found to happen since the gel mobility of the QDs is appreciably slowed down when conjugated with the DNA as compared to ssDNA (12 mer) and only QDs used as controls (Fig. 3A). DLS studies also revealed an increase in the average hydrodynamic radii from ~12 nm to ~21 nm after conjugation with DNA (supplementary information, Fig. S1). This is advantageous, since multiple attachments allow easy purification of the QD-DNA from the unreacted DNA by dialysis using suitable molecular weight cut off membrane. More importantly, a single QD with multiple DNA strands can self assemble multiple Pp IX-DNA conjugate, which can significantly increase FRET efficiency and hence ROS generation. This is one of the reasons, that QDs mediated FRET is worth exploring for photosensitization in PDT applications.

Pp IX has a two -COOH groups and thus has the possibility to conjugate itself with one or two ssDNA. For the conjugation of Pp IX to DNA, use of excess EDC and NHS leads to the

Physical Chemistry Chemical Physics Accepted Manuscript

activation of both the –COOH group in Pp IX, leading to the formation of Pp IX conjugate with single or two DNA strands. We used denaturing PAGE to visualize as well as to purify and isolate the Pp IX-DNA that contains only one DNA strand from the crude reaction mixture (Fig. 3B and S2). Attachment of Pp IX to the DNA modifies the gel mobility of the DNA strands, but two distinct bands were obtained corresponding to the number of DNA strands that were attached to the Pp IX molecule. The mobility of the Pp IX conjugated to one ssDNA band is less than the corresponding free 12 mer ssDNA but higher than the 24 mer ssDNA used as a control that confirmed the formation of Pp IX-DNA conjugate. The MALDI-TOF spectrum of purified Pp IX-DNA (supplementary information, Fig. S3) shows the base peak at 4546.09 corresponding to the mass of Pp IX-DNA. The UV-Visible, steady–state fluorescence and time resolved spectra of QD and Pp IX before and after conjugation with ssDNA shows insignificant differences in optical absorption and emission of the QD and Pp IX (supplementary information, Fig. S4 and S5).

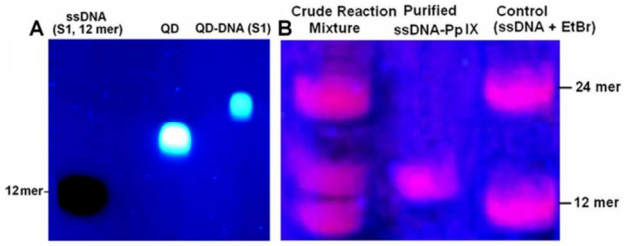

Fig. 3 **A.** Agarose gel image showing formation of QD-DNA conjugate. **B.** PAGE analysis of Pp IX-DNA conjugate.

The QD-DNA conjugate was hybridized with Pp IX–DNA conjugate through annealing. Since, multiple attachments of DNA strands with the QD was evident, we used four different concentrations of Pp IX-DNA conjugate (1:1 to 1:4) for the DNA hybridization. As the concentration of the Pp IX-DNA conjugate increases, chances of multiple assembly of Pp IX on a single QD also increase. From the gel image (Fig. 4 and S6) it can be seen that there is a retardation in the mobility of the band corresponding to the assembly as compared to dsDNA (12bp) and QD used as controls. With the increase in the reactant ratio of QD-DNA to Pp IX-DNA from 1:1 to 1:4, the retardation in gel mobility is more apparent. Moreover, the absence of any DNA other than the QD-DNA-Pp IX bands indicates that the hybridization is complete in the solution for both the samples.

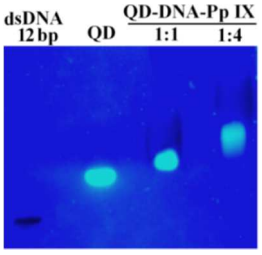

Fig. 4 Agarose Gel electrophoresis of QD-DNA-Pp IX assembly. S1-S2 was prestained with Sybr Green (Lane 1).

3.3. FRET Analysis

For efficient FRET to occur, the emission spectra of the donor should have a good overlap with the absorption spectra of the acceptor. ZnSe/ZnS QDs have an emission peak at 373 nm (band edge emission) and 450 nm (trap state emission) which shows good overlap with the soret band and Q bands of Pp IX respectively (supplementary information, Fig. S7). Absorption spectra of QD-Pp IX direct conjugate and QD-DNA-Pp IX assembly are shown in Fig. 5A and 6A respectively. The stoichiometry of the FRET probe (QD-Pp IX) formed by the direct conjugation and through DNA assembly was estimated from the absorption spectra and given in table 2.

FRET efficiency was calculated using the equations (3) and (4) for steady-state fluorescence measurement and excited-state lifetime decay of donor QD respectively:

$$E = 1 - F_{da}/F_d \quad (3)$$

$$E = 1 - \tau_{da}/\tau_d \quad (4)$$

Where F_d and F_{da} is the emission intensity of the donor QD in the absence and the presence of the acceptor Pp IX respectively, τ_d and τ_{da} are the excited-state lifetime of the donor QD in the absence and presence of the acceptor Pp IX respectively.

FRET analysis was done with two systems, QD-Pp IX direct covalent conjugate and QD-DNA-Pp IX assembled by DNA hybridization (with an increasing ratio of the Pp IX component). We studied the effect of the increasing ratio of the acceptor (Pp IX) at a constant concentration of the donor in each of the system. This ensures multiple attachment of the acceptor to a single QD. With an increasing ratio of the acceptor Pp IX a periodic decrease in the fluorescence intensity of the QDs was observed (Fig. 5B). FRET efficiency was found to increase from ca. 31% to 65% with the increase in the ratio of the QD:Pp IX from 1:0.88 to 1:2.88. However, no FRET was observed when solutions of QDs and Pp IX in the free state were mixed in the same ratio.

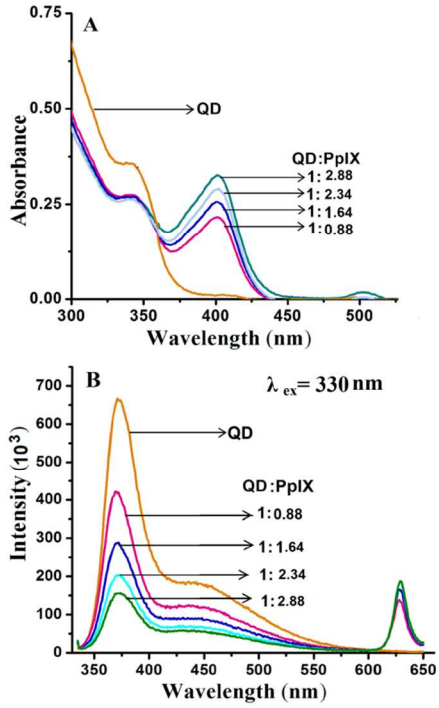

Fig. 5 **A.** UV-Visible absorption and **B.** Fluorescence Spectra of QD-Pp IX direct conjugate.

Physical Chemistry Chemical Physics Accepted Manuscript

In QD-DNA-Pp IX assembly there is an increase in the distance between QD and the photosensitizer Pp IX linked via 12 base pair DNA. Here also a periodic decrease in the fluorescence intensity of the QDs with the increasing concentration of Pp IX-DNA was observed by steady state measurement (Fig. 6B). FRET efficiency was found to increase from ca. 25% to 55% with an increase in the number of the Pp IX-DNA conjugate that is assembled to QD-DNA by hybridization. FRET depends on the distance between donor and acceptor molecules and their orientation. It is obvious that when QD and the Pp IX are assembled through DNA, the FRET efficiency decreases as evident from the data obtained in the current study (Table 2).

The FRET efficiency was also calculated from time resolved spectroscopy. The sample was excited using a 340 nm, 400 ps pulsed light emitting diode and the fluorescence decay profile of QDs was measured at emission wavelength of 373 nm. The fluorescence lifetime analysis software FluoFit professional of picoquant is used to analyse the results. Excited state lifetime of QDs was found to decrease on increasing the concentration of the Pp IX as shown in Fig. 7 which indicate a transfer of energy from donor to acceptor.[39] We observed decrease in the average lifetime of QDs from 55 ns to 22 ns on direct covalent conjugation with Pp IX (QD:Pp IX =1:2.88) and 24 ns for QD-DNA-Pp IX (QD-DNA:Pp IX-DNA=1:2.96) assembly. The FRET efficiency calculated from the time- resolved data have nearly the same values as calculated from the fluorescence intensity decay measurement (Table 2).

Table 2: Comparison of FRET efficiency calculated from steady sate and lifetime measurement of QDs.

FRET Efficiency from Steady State Fluorescence and Excited State Lifetime measurement of QD		
Ratio of product (QD: Pp IX)	**FRET Efficiency from Steady State**	**FRET Efficiency from Excited State Lifetime**
1:0.88	31 %	25 %
1:1.64	47 %	31 %
1:2.34	58 %	43 %
1:2.88	65 %	60 %

Ratio of product (QD-DNA: Pp IX-DNA)	**FRET Efficiency from Steady State**	**FRET Efficiency from Excited State Lifetime**
1:0.85	25 %	20 %
1:1.64	32 %	30 %
1:2.40	43 %	44 %
1:2.96	55%	57 %

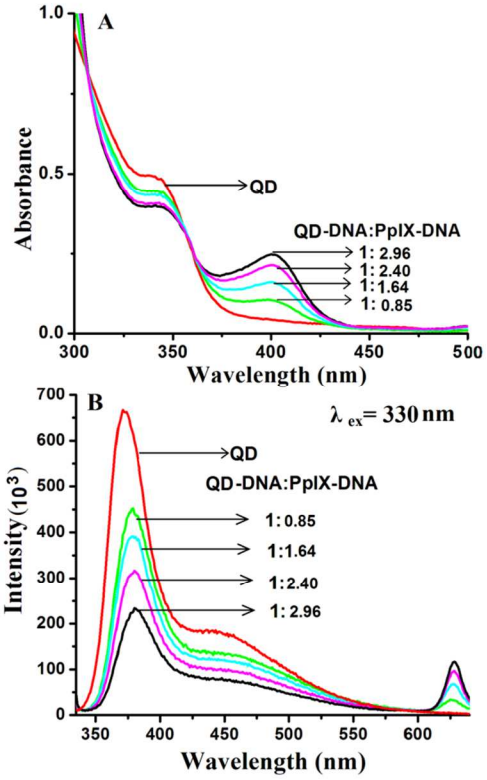

Fig. 6 **A.** UV- Visible absorption and **B.** Fluorescence Spectra of QD-DNA-Pp IX assembly.

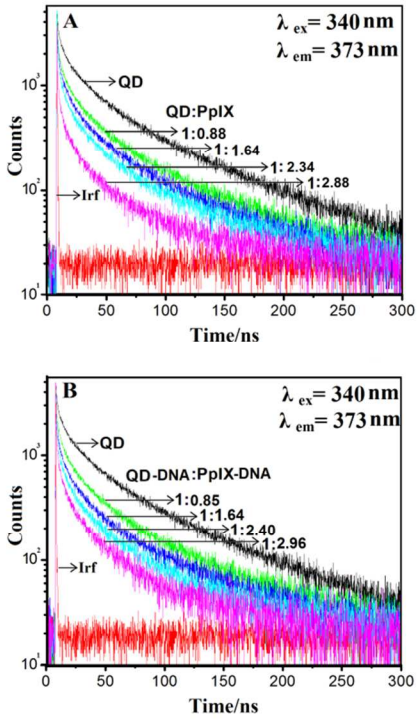

Fig. 7 Time-resolved fluorescence decay of **A.** QD-Pp IX Conjugate and **B**. QD-DNA-Pp IX assembly recorded for solutions with varying ratio of donor and acceptor. Irf: Instrument Respose Function.

Physical Chemistry Chemical Physics Accepted Manuscript

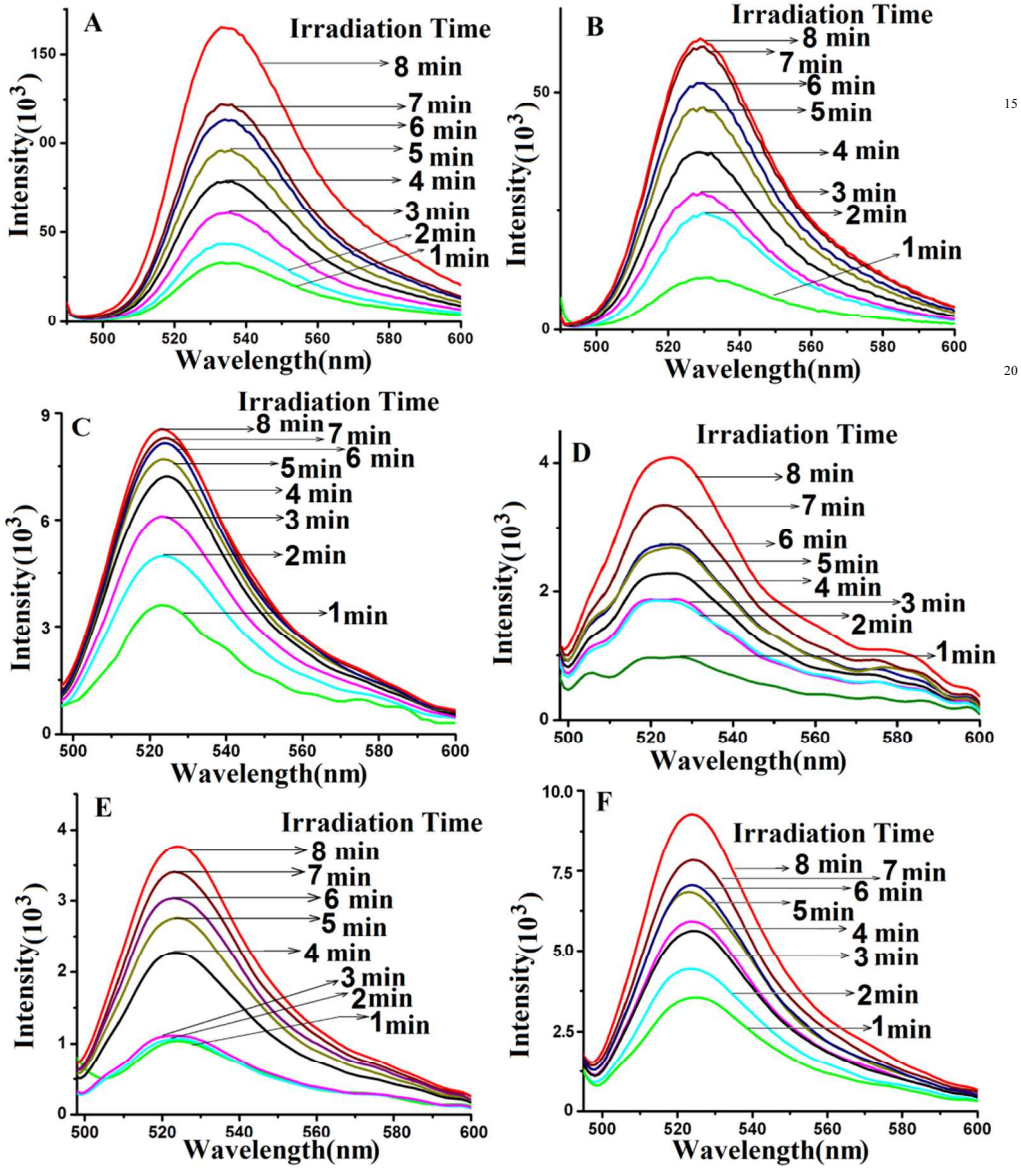

Fig. 8 Rhodamine 123 Fluorescence Emission at λex = 485 nm due to ROS generation in **A.** QD-Pp IX direct conjugate **B.** QD-DNA-Pp IX assembly **C.** QD and Pp IX in free state **D.** QD-DNA and Pp IX-DNA in free state **E.** QD only and **F.** Pp IX only.

3.4. Kinetics of ROS Formation

Irradiation of QDs with UV light in dark leads to the excitation of the QDs. The QD transfers its energy to the acceptor Pp IX generating excited molecules of Pp IX. The excited Pp IX gets de-excited by energy transfer to neighboring oxygen molecules to form ROS. The decay of Pp IX features in the absorption spectra (Fig. S8 and S9) occurs due to the photooxidation of Pp IX and is indicative of the formation of ROS.[40, 41] The resultant ROS can be monitored by its emission at 1270 nm. However, the short lifetime of ROS in the nanosecond range makes it difficult to estimate it quantitatively. For this purpose, dihydrorhodamine 123 (DHR 123), a universal ROS tracking agent is generally used for ROS measurement.[15] The nonfluorescent DHR 123 gets converted into fluorescent rhodamine 123 on oxidation by the ROS and emit at ~ 530 nm.

The ROS generation was studied for the free QDs, free Pp IX, QD-S1, QD-S1-S2 (QD conjugated to S1 and S1 annealed to S2), Pp IX-S2, PpIX-S2-S1, mixture of QDs and Pp IX in the free state without any conjugation, mixture of QD-S1 and Pp IX-S2 in free state without hybridization, QD-Pp IX direct conjugate and QD-S1-S2-Pp IX assembly (Fig. 8, S8-S12). For ROS generation study of the FRET probes, samples in different ratios have been used. All the samples were analysed before

Physical Chemistry Chemical Physics Accepted Manuscript

and after irradiation of samples on addition of DHR 123. The presence of absorbance peak at 500 nm and emission peak at ~ 530 nm at excitation wavelength of 485 nm confirms the formation of rhodamine 123 from DHR 123 due to ROS generation (supplementary information Fig. S8-S12). The fluorescence from rhodamine 123 (λ_{max} ~ 530 nm) for different time intervals was measured spectrophotometrically. It can be seen from the absorbance (500 nm) and fluorescence peak (~530 nm) of rhodamine 123 (Fig. 8 and S8-S12) that the samples containing FRET probes show higher ROS generation as compared to the free QD, QD-S1, QD-S1-S2, free Pp IX, Pp IX-S2, Pp IX-S2-S1, mixture of QDs and Pp IX in the free state without any conjugation, mixture of QD-S1 and Pp IX-S2 in free state without hybridization. The photosensitizer Pp IX in the free state does not get sufficient energy for excitation and hence leads to less ROS generation. The same is true for PpIX-S2 conjugate in single or duplexed with S1 strand. As expected, ROS generation from QD-Pp IX direct conjugate is the highest among all the samples followed by the QD-DNA-Pp IX assembly. This is due to more efficient FRET in the former that leads to the formation of increased amounts of ROS as compared to the QD-DNA-Pp IX assembly, where the acceptor and the donor are separated in space by a 12-mer duplex DNA. Nevertheless, the QD-Pp IX direct conjugate lacks the biorecognition and possible targeting entity which is present as DNA in the current study. This DNA strand is open to modification and can be wisely chosen to target various cell surface markers, that will increase the efficiency of the treatment modality as in PDT.

4. Conclusion

Water soluble, non-toxic QDs can serve the dual purpose of imaging and a FRET donor for the generation of ROS for potential application in PDT. Conjugated with DNA, they can be self assembled with photosensitizers and directed to specific tissues for imaging and targeted destruction of diseased cells. Herein, ZnSe/ZnS QDs was synthesized and conjugated to ssDNA using EDC-NHS mediated amide formation chemistry. Same chemistry was used to conjugate the photosensitizer Pp IX with ssDNA that is complementary to the DNA attached to the QD. The self-assembly of the QD-DNA conjugate and the Pp IX-DNA conjugate was achieved by hybridization of the DNA strands. FRET efficiency was compared with various models that include direct covalent conjugate of QDs- Pp IX, and QD-DNA-Pp IX assembly, where the QD was the donor and the Pp IX was the acceptor. As a proof of principle, ROS generation was also compared with the two models along with the individual entities in solution. A significant and systematic increase in the ROS formation was observed for the QD-Pp IX direct conjugate as well as the QD-DNA-Pp IX assembly as compared to the individual species in solution. We postulate that with the careful manipulation of the DNA sequence, the donor and the acceptor, the assembly of QD-DNA-photosensitizer can have general applicability, in particular in PDT with the dual purpose of imaging and targeted, controlled release of ROS for the treatment of relevant cancers.

Acknowledgements

This work was supported by a grant to P. D., S. H. and M. K. Singh from BRNS, Department of Atomic Energy (DAE), Govt. of India, Project No. 2012/34/59/BRNS. S.S. and V. S. are thankful to BRNS and CSIR, India for fellowship. S. H. is also thankful to DST for grant (SR/FT/CS-093/2009). Authors are thankful to IIT Patna, BARC (Mumbai) and IIT Madras for infrastructure and experimental facilities.

Notes and references

[a]*Department of Chemistry, Indian Institute of Technology, Patna, Patna- 800013, Bihar, India. Email: prolay@iitp.ac.in; Fax: +91 612 225 7383, Tel: +91 612 255 2057*

[b]*Indian Institute of Science Education and Research Kolkata, West Bengal, India.*

[c]*Atomic and Molecular Physics Division, Bhabha Atomic Research Centre, Mumbai -400094, India. Email:mksingh @barc.gov.in; Fax: +91 -22-2550 5151, Tel: +91-22-2559 3987*

Electronic Supplementary Information (ESI) available: Dynamic light scattering of ZnSe/ZnS QD and QD-DNA conjugate, gel images, MALDI-TOF spectra of Pp IX-DNA conjugate, UV-Visible and fluorescence spectra of QD and Pp IX before and after conjugation with DNA, the Overlap spectra of QD (donor) and Pp IX (acceptor) and comparative UV-Visible and fluorescence spectra for ROS generation in various systems of QD and Pp IX. See DOI: 10.1039/b000000x/

1 L. Bonacina, *Mol. Pharmaceutics*, 2013, **10**, 783−792.
2 M. Goldberg, R. Langer and X. Jia, *J. Biomater. Sci. Polym. Ed*., 2007, **18**, 241–268.
3 C. Tassa, S. Y. Shaw and R. Weissleder, *Acc. Chem. Res*., 2011, **44**, 842-852.
4 D. Geißler, S. Linden, K. Liermann, K. D. Wegner, L. J. Charbonnière and N. Hildebrandt, *Inorg. Chem*., 2014, **53**, 1824−1838.
5 P. R. Gil and W. J. Parak, *ACS Nano*, 2008, **2**, 2200-2205.
6 A. Gajewicz, T. Puzyn, B. Rasulev, D. Leszczynska and J. Leszczynski, *Nanoscience and Nanotechnology-Asia*, 2011, **1**, 53-58.
7 A. Prakash and D. Bahadur, *Phys. Chem. Chem. Phys.*, 2014, **16**, 21429-21437.
8 C. M. Tyrakowski and P. T. Snee, *Phys. Chem. Chem. Phys.*, 2014, **16**, 837.
9 S. K. Muzakir, N. Alias, M. M. Yusoffab and R. Jose, *Phys. Chem. Chem. Phys*., 2013, **15**, 16275-16285.
10 P. Juzenasa, W. Chenb, Y. P. Sunc, M. A. N. Coelhod, R. Generalova, N. Generalovaa and I. L. Christensena, *Adv. Drug Deli. Rev.*, 2008, **60**, 1600–1614.
11 T. R. Pisanic, Y. Zhangb and T. H. Wang, *Analyst*, 2014, **139**, 2968-2981.
12 J. Liab and J. J. Zhu, *Analyst*, 2013, **138**, 2506-2515.
13 A. Smith, S. Dave, S. Nie, L.True and X. Gao, *Expert Rev. Mol. Diagn.*, 2006, **6**, 231-244.
14 C. Fowley, N. Nomikou, A. P. McHale, B. McCaughana and J. F. Callan, *Chem. Commun.*, 2013, **49**, 8934.
15 M. Oo, Y. Yang, Y. Hu, M. Gomez, H. Du and H. Wang, *ACS Nano*, 2012, **6**, 1939-1947.
16 Y. Chenga, J. D. Meyersa, A. M. Broome , M. E. Kenney, J.P. Basilion and C. Burdab, *J. Am. Chem. Soc*., 2011, **133**, 2583–2591.
17 H. M. E. Azzazy, M. M. H. Mansour and S. C. Kazmierczak, *CLB.*, 2007, **40**, 917-927.

Physical Chemistry Chemical Physics Accepted Manuscript

18 L. Shao, Y. Gao and F. Yan, *Sensors*, 2011, **11**, 11736-11751.

19 A. C. S. Samia, X. Chen and C. Burda, *J. Am. Chem. Soc*., 2003, **125**, 15736-15737.

20 Y. J. Choi1, Y. J. Kim, J. W. Lee, Y. Lee, Y. Lim and H. W. Chung, *J. Nanosci. Nanotechnol.*, 2012, **12**, 2160-2168.

21 A. A. Anas, H. Akita, H. Harashima, T. Itoh, M. Ishikawa and V. Biju, *J. Phys. Chem., B*, 2008, **112**, 10005–10011.

22 S. J. Soenena, P. Gil, J. M. Montenegrob, W. J. Parakb, S. C. De Smedta, K. Braeckmansa, *Nano Today*, 2011, **6**, 446-465.

23 A. Valipoor, K. Parivar, M. Modaresi, M. Messripour, *Nanomed.*, 2014, **1**, 258-265.

24 K. Kim, S. Kim, S. Beck, J. Yang, S. Yuan, S. Hahn, *Nanomed-Nanotechnol.,* 2012, **8**, 1070-1073.

25 Y. Bae and K. Park, *J. Control Release*, 2011,**153**, 198-205.

26 D. J. Adams, Z. V. Boskovic, J. R. Theriault, A. J. Wang, A. M. Stern, B. K. Wagner, A. F. Shamji and S. L. Schreiber, *ACS Chem. Biol*., 2013, **8**, 923−929.

27 R. A. Cairns, I. S. Harris and T. W. Mak, *Nat. Rev. Cancer*, 2011, **11**, 85-95.

28 D. Trachootham, J. Alexandre & P. Huang, *Nat. Rev. Drug Discov.*, 2009, **8**, 579-591.

29 A. Accardo, D. Tesauro and G. Morelli, *Polym. J.*, 2013, **45**, 481-493.

30 M. Yu, J. Park and S. Jon, *Theranostics,* 2012, **2**, 3-44.

31 H. Had, M. Roh, A. Giani, T. Hisatomi, S. Nakao, I. K. Kim, E. S. Gragoudas, D. Vavvas, S. Guccione, J. W. Miller, *Plos One*, 2011, **6**, e18864.

32 A. K. H. Cheng, H. Su, Y. A. Wang and H.Z. Yu, *Anal. Chem*., 2009, **81**, 6130–6139.

33 H. Qian, X. Qiu, L. Li and J. Ren, *J. Phys. Chem. B.*, 2006, **110**, 9034-9040.

34 A. Aboulaich, M. Geszke, L. Balan, J. Ghanbaja, G. Medjahdi and R. Schneider, *Inorg. Chem.,* 2010, **49**, 10940–10948.

35 Q. Liang, Y. Bai, L. Han, X. Deng, X. Wu, Z. Wang, X. Liu and J. Meng, *JOL.*, 2013, **143**, 185-192.

36 C. Shen and W. L. Tseng, *Inorg. Chem.*, 2009, **48,** 8689–8694.

37 S. Karasawa, T. Araki, T. Nagai, H. Mizuno and A. Miyawaki, *Biochem. J.*, 2004, **381**, 307–312.

38 D. Bartczak and A. G. Kanaras, *Langmuir*, 2011, **27**, 10119–10123.

39 S. Sarkar, R. Bose, S. Jana, N. Jana and N. Pradhan, *J. Phys. Chem. Lett.*, 2010, **1**, 636–640.

40 R. Rotomskis, S. Bagdonas and G. Streckyte, *J. Photochem. Photobiol. B, Biol.*, 1996, **33**, 61-61.

41 P. Juzenas, S. Sharfaei, J. Moan and R. Bissonnette, *J. Photochem. Photobiol. B, Biol*., 2002, **67**, 11-17.

Physical Chemistry Chemical Physics Accepted Manuscript